https://doi.org/10.1016/j.orgel.2021.106307

Thermally Stable Inverted Organic Light-emitting Diodes using Ag-doped 4,7-Diphenyl-1,10-phenanthroline as an Electron Injection Layer

Chunliu Gong[a], Yachen Xu[b], Yuling Liu[a], Yingjie Liao[b], Weixia Lan[b], Bin Wei[a,b,*], Lian Duan[c,**], Wai-Yeung Wong[d,***]

[a]School of Materials Science and Engineering, Key Laboratory of Advanced Display and System Applications, Ministry of Education, Shanghai University, China

[b]School of Mechatronic Engineering and Automation, Shanghai University, Shanghai, 200444, China
E-mail: bwei@shu.edu.cn

[c]Key Laboratory of Organic Optoelectronics and Department of Chemistry, Tsinghua University, Beijing 100084, China
E-mail: duanl@mail.tsinghua.edu.cn

[d]Department of Applied Biology and Chemical Technology and Research Institute for Smart Energy, The Hong Kong Polytechnic University, Hung Hom, Kowloon, Hong Kong, China
E-mail: wai-yeung.wong@polyu.edu.hk

Keywords：silver-doped, inverted organic light-emitting diodes, grazing incidence small angle X-ray scattering, thermal stability, annealing

Abstract: The thermal stability of organic functional materials affects the

performance and lifetime of organic light-emitting diodes (OLEDs). We have developed a thermally stable inverted OLEDs (IOLEDs) by employing silver (Ag) doped into 4,7-diphenyl-1,10-phenanthroline (Bphen) as an *n*-type doped electron injection layer (EIL). We found that the formation of Ag complexes by coordination reaction could enhance the thermal stability and produce an asymmetric diffraction pattern based on an analysis of grazing incidence small angle X-ray scattering. Interestingly, with the annealing temperature increasing to 100 ℃, the electrical properties of electron-only cells show differentiated phenomenon that the current density based on Ag dopant remains basically unchanged, which is opposite to Cs_2CO_3 dopant. In addition, at the high temperature of 100 ℃, the IOLEDs with Cs_2CO_3 doped Bphen as an EIL was damaged completely, while the Ag dopant-based devices still maintained good photoelectrical characteristics. Finally, we have demonstrated that the optimized IOLEDs achieved a 40.3% enhancement in current efficiency compared to the conventional device. This work provides a new strategy to increase the thermal stability and performance for the application of IOLEDs operated under high temperature.

1. Introduction

Organic light-emitting diodes (OLEDs) have shown great potential in the field of display and solid-state lighting due to their low price, low weight, and flexibility since their discovery [1-5]. Inverted OLEDs (IOLEDs) have attracted more and more

attention because they are easier to integrate with *n*-type oxide thin film transistor or low-temperature polysilicon [6,7]. However, the high turn-on voltage and insufficient thermal stability of IOLEDs have restricted its future development. Although there have been many studies on improving the electrical performance of IOLEDs to date, there are still less attention on their thermal stability. Generally, IOLEDs have good air stability because the electron transport materials sensitive to water and oxygen are protected at the bottom of the other organic layers. However, it is well known that 4,7-diphenyl-1,10-phenanthroline (Bphen), as an excellent electron transport material, has been widely used in various IOLEDs, while its low glass transition temperature ($T_g \approx$ 62 ℃) [8] leads to a poor thermal stability. It has been reported that phenanthroline derivatives can form metal complexes with a variety of metals and their metal compounds [9-13]. However, the effect of improving the performance and thermal stability of OLEDs varies greatly with different species of metal [9]. Furthermore, some research works reported a variety of phenanthroline derivatives with better electron transport ability and higher thermal stability [10]. This metal-doped phenanthroline derivatives system has gradually open a new strategy to increase the thermal stability of OLEDs. However, its application in IOLEDs at high temperature is still relatively insufficient.

On the other hand, the work function (WF) of indium tin oxide (ITO) is about 4.8 eV, however, the lowest unoccupied molecular orbital (LUMO) energy level of most organic materials is about 2.5 eV to 3.5 eV, which will result in a big energy barrier [14,15]. As such, the huge energy barrier gap between the cathode ITO and the electron

transport layer (ETL) is the main reason hindering the excellent performance of IOLEDs. Some researchers have proposed some approaches to realizing the efficient electron injection capability of IOLEDs as follows: (i) A variety of materials such as low-WF zinc oxide, tin dioxide, and ultra-thin Alq_3-LiF-Al trilayer, can be used as an electron injection layer (EIL) [16-18]; (ii) The ultra-thin Al and metal sulphide can be used to modify the cathode ITO of IOLEDs, thus reducing the electron injection barrier to improve the photoelectric performance and enhance the stability of IOLEDs [19-21]; (iii) The *n*-type doped structure as an EIL can be employed to improve the electron injection ability and balance the carrier injection, such as Cs_2CO_3-doped Bphen [22-24]. Such strategies have a good effect on solving the poor device performance of IOLEDs.

Here, we used Ag doping into the Bphen film as an EIL in the IOLEDs to enhance the device thermal stability and performance. Bphen is of excellent electron-transporting and hole-blocking abilities. In addition, Bphen can undergo coordination reactions with metals to improve thermal stability. Comparing with other species of metals, Ag as dopant was found to produce stronger complex compound with Bphen. The thermal stability of Ag-doped Bphen system was investigated in terms of the changes in its film morphology, the electrical properties of electron-only cells (EOCs) and photoelectric properties of IOLEDs after annealing. In addition, the analysis of grazing incidence small angle X-ray scattering (GISAXS) can further elucidate the reasons for the increase in thermal stability. Finally, the Bphen films with different Ag-doped ratio as an EIL in IOLEDs have been studied.

2. Experimental

The hole-transporting materials of N,N′-di(naphth-1-yl)-N,N′-diphenyl-benzidine (NPB) and 4,4′,4-tris(carbazol-9-yl)triphenylamine (TCTA), the electron transporting material of Bphen and 4,6-bis(3,5-di(pyridin-3-yl)phenyl)-2-methylpyrimidine (B3PYMPM) were obtained from Sigma Aldrich Co. Ltd. The green luminescent material 8-hydroxyquinoline aluminum salt (Alq_3) and the blue luminescent material 4-di-[4-(N,N-diphenyl)amino] styryl-benzene (DSA-ph) were obtained from Lumtec Corp. The thickness of an indium tin oxide (ITO) coated glass substrate is 180 nm and the square resistance is 10 Ω/sheet.

As shown in Fig. S1 (a), a structural diagram of green IOLEDs (reference devices 0, G-1, G-2, G-3, G-4, G-5): indium tin oxide (ITO)/Bphen: χ wt% Ag (10 nm)/Bphen (30 nm)/Alq_3 (20 nm)/NPB (40 nm)/MoO_3 (5 nm)/Al (150 nm), where χ are 0, 5, 10, 15, 20 and 40, respectively, were fabricated to investigate the optimized doping ratio for achieving better performance. In addition, the blue IOLEDs with the configuration of ITO/EIL (30 nm)/B3PYMPM (10 nm)/ADN: 5 wt% DSA-ph (20 nm)/TCTA (40 nm)/MoO_3 (5 nm)/Al (150 nm), where EILs are Cs_2CO_3 or Ag doped Bphen, respectively, were fabricated to investigate the thermal stability. The organic materials used have high thermal stability (TCTA, T_g=152 ℃, B3PYMPM and ADN have no obvious T_g).

The patterned ITO glass substrates were cleaned in an ultrasonic bath with de-ionized water, acetone and isopropanol consecutively, and then treated by ultraviolet

ozone for 5 minutes. Then, organic functional layers are sequentially vapor-deposited into a high-vacuum chamber (1×10^{-6} mbar). The device active area was 0.04 cm^2 defined by crossing area of cathode and anode. The deposition rates of organic materials and Al anode were 1.0 Å/s and 5.0 Å/s, respectively. The evaporation rate of Ag and Bphen are approximately 0-0.4 Å/s and 1.0 Å/s, respectively, under the respective density options. The film thickness is monitored by a quartz balance during evaporation.

The changes of film morphology under different annealing conditions were studied by atomic force microscopy (AFM, BioScope Resolve, Bruker). The samples of the barrier film were thermally deposited on the glass substrate for the grazing incidence small angle X-ray scattering (GISAXS) measurements at the Shanghai Synchrotron Radiation Facility. The electrical characteristics of electronic only cells (EOCs) were investigated by Keithley2400 Sourcemeter (Keithley Instruments, Inc., Cleveland, OH, USA). The PR650 spectral colorimeter (Photo Research, Inc., Chatsworth, CA, USA) was used to describe the changes of electroluminescence characteristics of green and blue IOLEDs.

All measurements were performed in an atmospheric environment without encapsulation. In order to maintain the authenticity of the data, all data were averaged.

3. Results and discussion

3.1. The morphologies of neat and doped Bphen films with and without annealing

The morphologies of different films deposited on ITO glass after annealing at

different temperatures as shown in Fig. 1. Those morphologies (Fig. 1 (a)) show that the neat Bphen has very good film flatness, but the film flatness of Cs_2CO_3-doped Bphen (RMS = 0.6012 nm) and Ag-doped Bphen (RMS = 1.4610 nm) is significantly reduced before annealing. The Cs_2CO_3 and Ag particles lead to an increase in roughness and Ag-doped Bphen film has higher roughness due to the larger size of Ag particles than Cs_2CO_3. On the other hand, the reasonable increase in roughness of the organic functional layer is beneficial to increase the interface contact area of adjacent layers. The stronger carrier injection capability helps to achieve a greater number of excitons recombined, so a higher current efficiency of the device can be obtained.

The high temperature environment can induce crystallization of organic materials, while the T_g of Bphen ($T_g \approx 62$ ℃) is low. Therefore, OLEDs with the neat Bphen are difficult to maintain stability in a high temperature environment. Figure 1s (b) and (c) display the changes of the film morphology based on Cs_2CO_3 and Ag doped Bphen after annealing at 60, 80 and 100 ℃, respectively. The surface roughness of the film based on Cs_2CO_3 increases with the continuous annealing temperature and the surface crystallization phenomenon occurs when annealed at a temperature of 100 ℃. However, as a contrast, the film morphology based on Ag dopant does not appear to show breakdown or interface crystallization before and after annealing at different temperatures. Thus, it reveals that Ag-doped Bphen system can greatly suppress the change of the film morphology and improve the device thermal stability.

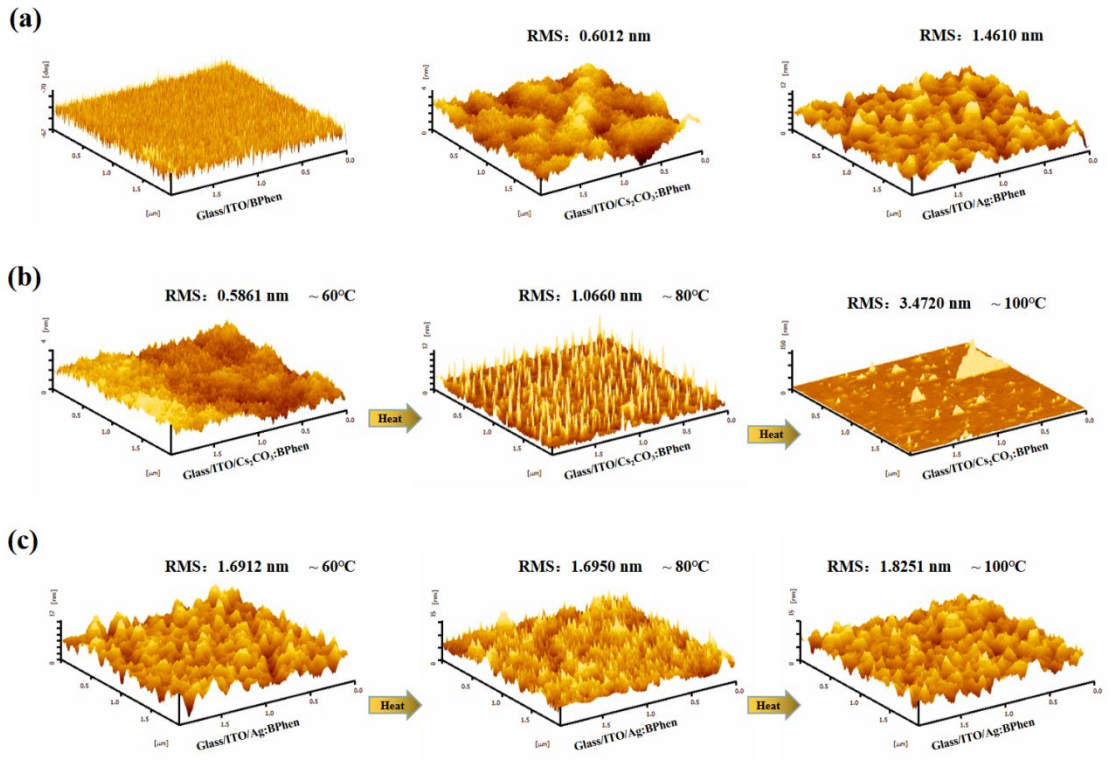

Fig. 1. The AFM images of different films of 60 nm thickness deposited on ITO glass after annealing for 60 minutes. (a) The morphologies of three different structures (the neat Bphen, Cs_2CO_3-doped Bphen and Ag-doped Bphen films) in an atmospheric environment at RT. The film morphologies of Cs_2CO_3-doped Bphen (b) and Ag doped Bphen (c) after annealing at 60, 80 and 100 °C.

To further analyze the characteristics of the three different structures of the film, we carried out GISAXS characterization on them. Figure 2s (a), (b) and (c) illustrate the GISAXS patterns (original and enlarged) and the schematic of molecular distribution of three different films of neat Bphen, Cs_2CO_3 doped Bphen and Ag doped Bphen, respectively. As shown in Fig. 2, the Cs_2CO_3 and Ag-doped films have stronger diffraction spots compared to the neat Bphen film. This can be caused by the formation of metal complexes, which changed the tightly packed molecular arrangement. Some

research studies reported that the scattering intensity of the Ag-doped Bphen film in the q_z direction was smaller than that of Cs_2CO_3-doped Bphen film [25-28], indicating that the layer structure became dominant. As for the obvious semicircular scattering intensity distribution of Ag-doped Bphen film (Fig. 2(c) pointed by the arrow), we speculate that this phenomenon is closely related to the bigger roughness and stronger diffuse reflection effect caused by the aggregation effect of excessive Ag particles.

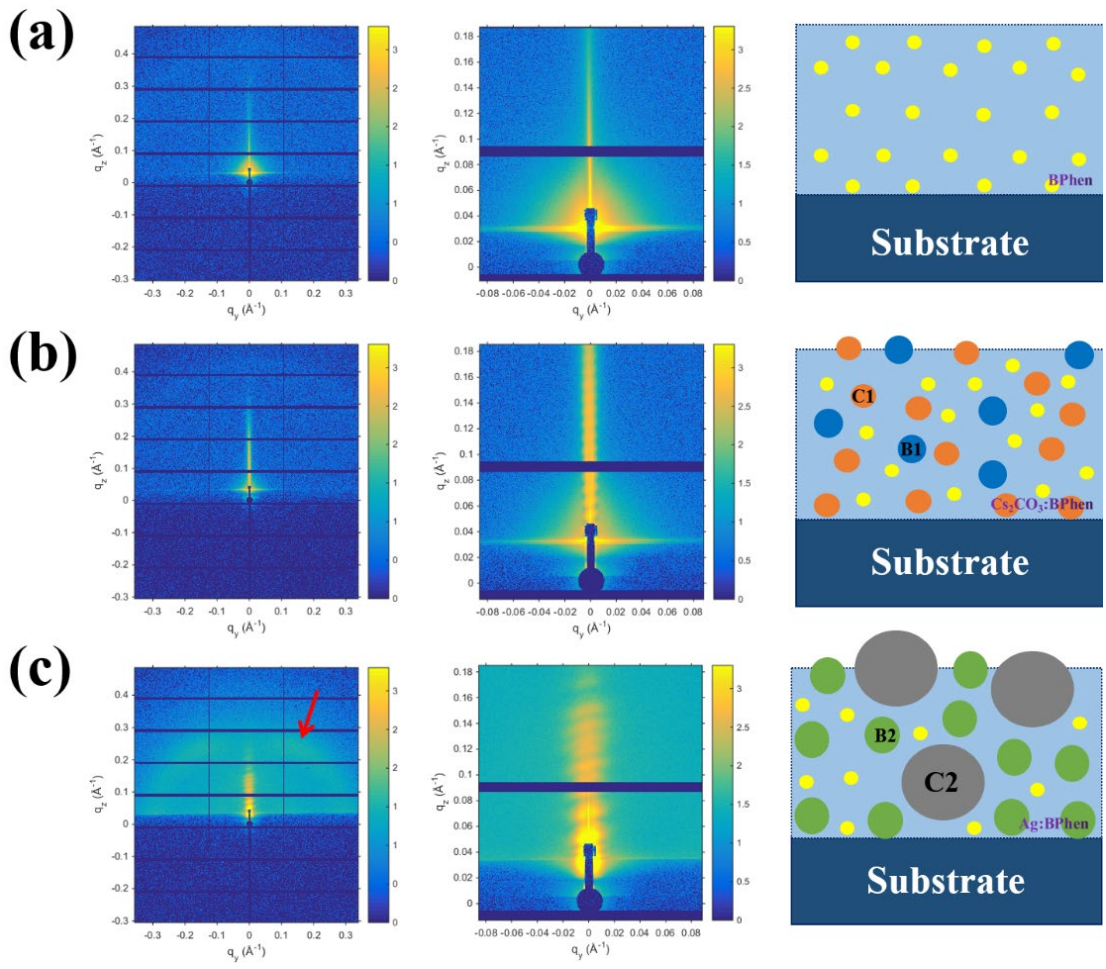

Fig. 2. The GISAXS patterns: original (column 1), enlarged (column 2) and the schematic of molecular distribution (column 3) of different films. (a) The neat Bphen. (b) Cs_2CO_3 doped Bphen and (c) Ag doped Bphen. Note: B1 and B2 represent the complexes of Cs and Ag, respectively. C1 and C2 represent the Cs salt particles and

metallic Ag particles, respectively. Due to the aggregation effect of Ag particles, its size is larger than that of Cs salt.

3.2.The electrical performance of EOCs after annealing

Furthermore, to explore the thermal stability of the organic functional layer with the Cs_2CO_3 or Ag dopant in the Bphen matrix, we further studied the electrical characteristics of the EOCs with different dopants in the Bphen matrix at different temperatures (room temperature (RT), 60, 80 and 100 °C). The structures of EOCs are ITO/10 wt% Ag or Cs_2CO_3: Bphen(30 nm)/B3PYMPM(60 nm)/LiF(1 nm)/Al(150 nm), among which B3PYMPM has no obvious T_g [29]. Two different EOCs were annealed at different temperature for 4 hours and its voltage was recorded from 0 to 5 V corresponding to the current density changes. After annealing at 60, 80 and 100 °C for 240 minutes, as shown in Fig. 3s (a), (b) and (c), respectively, the Cs_2CO_3-doped Bphen EOCs exhibit a multiple increase in the current density of 80 and 100 °C. However, the overall current density of the EOCs with Ag-doped Bphen as an EIL remains basically unchanged after annealing at 60, 80 and 100 °C for 240 minutes, as shown in Fig. 3s (d), (e) and (f), respectively. These results are consistent with the changes of the film morphology in Fig. 1 (b), indicating that thermal annealing will induce the reorganization of organic molecules and promote crystallization. Therefore, we conclude that the film with Ag dopant in the Bphen matrix has a better thermal stability.

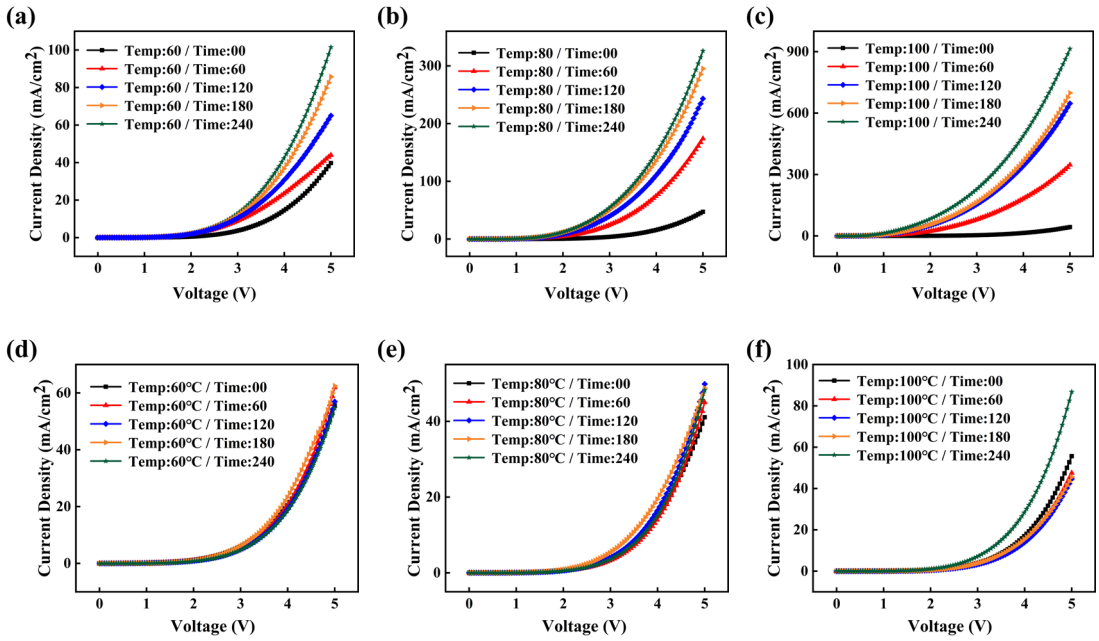

Fig. 3. The current density versus voltage (*J-V*) of two types of EOCs (ITO/Bphen: 10 wt% (Ag or Cs_2CO_3): Bphen (30 nm)/B3PYMPM (60 nm)/LiF (1 nm)/Al (150 nm)) at different temperatures and times. (a) Cs_2CO_3-doped Bphen at 60 ℃. (b) Cs_2CO_3-doped Bphen at 80 ℃. (c) Cs_2CO_3-doped Bphen at 100 ℃. (d) Ag-doped Bphen at 60 ℃. (e) Ag-doped Bphen at 80 ℃. (f) Ag-doped Bphen at 100 ℃.

High-temperature annealing will cause the molecular structure of low-T_g materials to be more regular, so that the current density increases sharply. Although the device structure based on Cs_2CO_3-doped Bphen reported in the literature still has good thermal stability at 80 °C [11], the erosion of water and oxygen will further cause its film to be more easily damaged due to the annealing in the atmosphere. Moreover, high temperature will aggravate the diffusion of Cs^+, thereby greatly increasing the electron injection capability. According to Fig. 4, after annealing at different temperatures (60, 80 and 100 °C) for one hour, the EOCs based on Ag-doped Bphen exhibit an excellent

thermal stability.

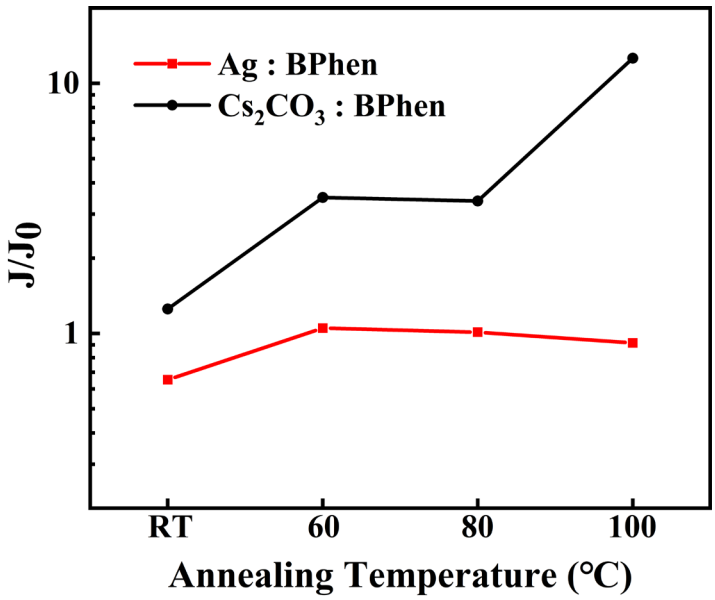

Fig. 4. The normalized current densities of the two types of EOCs versus the annealing temperature after annealing at a 5 V bias voltage for one hour.

3.3.The optoelectronic performance and thermal stability of IOLEDs

As illustrated in Fig. S1 (b), there is an energy barrier of about 1.8 eV between the WF of ITO and the LUMO energy level of Bphen, so that the performance of the IOLEDs without inserting an EIL is very poor (Fig. S2 and Table S1). The turn-on voltage of reference device 0 is about 13 V and the luminance is low (Fig. S2 (a)). Moreover, the max external quantum efficiency (EQE_{max}) and the max power efficiency (PE_{max}) are 1.46% and 0.63 lm W^{-1}, respectively (Fig. S2 (b)). Therefore, the widely used solution is to employ metal Cs or Cs_2CO_3 doped Bphen as an EIL, which helps to promote the electron injection ability and balance the hole-electron pairs. By doping Cs_2CO_3 into Bphen (reference device 3), the turn-on voltage drops dramatically from 13 V to 3.2 V and the maximum current efficiency (CE_{max}) increased to 4.89 cd A^{-1}.

Moreover, PE_{max} increased to 2.90 lm W^{-1}, which are about 5-times higher than reference device 0 due to the drastic reduction of the driving voltage. Here, we propose an alternative strategy to solve the poor electrical performance problem of IOLEDs due to the excessively high energy barriers using metal Ag-doped Bphen as an EIL. As shown in Fig. S3 and Table S1, the best performance among Ag-doped Bphen as an EIL in IOLEDs was explored by optimizing the doping ratio. Device G-3 with Ag doping ratio of 15% exhibits a superior performance to other devices, as seen in Fig. S3, in which its operation bias is the lowest under the same current density (Fig. S3 (a)). In addition, the turn-on voltage, the CE_{max} and the PE_{max} of Device G-3 are 3.6 V and 5.91 cd A^{-1}, as observed from Fig. S3 (b) and Fig. S3 (c), respectively.

On the one hand, the metal complex formed by the coordination reaction between the metal Ag and Bphen can reduce the LUMO energy level, thereby enhancing the electron injection to improve the device performance [30]. The interaction between Bphen molecules and Ag tends to combine with Ag^+ to form $[Ag(Bphen)^+]$ and $[Ag(Bphen)_2]^+$, thereby promoting the balance between organic ligands and metal ions to move in the positive direction so that free electrons are more easily released, which can promote electron injection [9]. In addition, Ag particles doping into the Bphen film can easily cause a strong local surface plasmon effect, resulting in three meaningful effects: (i) suppress surface plasmon primitive (SPP) mode loss, (ii) adjust the energy level to lower the electron injection barrier and (iii) induce and enhance local surface plasmon resonance coupling electric field [31]. The light scattering effect caused by the metallic Ag particles also helps to capture the luminous flux to further improve the

device efficiency. Secondly, since the local electric field can be approximately described as $\boldsymbol{E} = \frac{\boldsymbol{Q}}{\boldsymbol{4\pi\varepsilon R^2}}$, it shows that small size Ag particles can increase the local electric field strength, which makes the injection of electrons easier and lowers the driving voltage. This explains why the devices with a higher doping ratio of Ag actually decrease the overall device performance. The reason is that Ag particles tend to agglomerate and cause their size to increase. As shown in Fig. S3 (d), its peak emission keeps basically unchanged, but its corresponding full width at half maximum is slightly reduced with the continuous increase of the doping ratio of Ag, especially at the 40% doping ratio. We assume that the phenomenon is also caused by the local surface plasmon effect [32].

Figure S4 shows the performance of the conventional devices with and without MoO_3. Although MoO_3 contributes to the enhancement of hole injection, the hole transport of organic materials is inherently superior to the electron transport ability, thus, the addition of MoO_3 is easier to cause the imbalance of charge carrier injection. Therefore, although the device with MoO_3 has a higher current density (Fig. S4 (a)), its CE_{max} and EQE_{max}, as respectively illustrated in Fig. S4s (b) and (c), are relatively lower. It is worthy to note that the electroluminescence (EL) spectra for both devices keep basically unchanged (Fig. S4 (d)).

Here, we used a device structure without MoO_3 (reference device 1) which has a high CE as the conventional comparison to G-3 and reference device 3 with Ag and Cs_2CO_3 doped, respectively. As shown in Fig. 5s (a), (b) and Table S1, the turn-on voltage of the conventional device (reference device 1) is 2.6 V, while the turn-on

voltages of the inverted device (reference device 3 and G-3) are 3.2 V and 3.6 V, respectively. This phenomenon is caused by the high electron injection barrier of the inverted structure itself and can be further optimized using double EILs [19-21]. For G-3, CE_{max} is 5.91 cd A^{-1}, which is 40.3% higher than reference device 1 in Fig. 5 (c). Although the current density and luminance of the inverted device reference device 3 are better than Ag doped G-3, its CE_{max} is only 4.89 cd A^{-1}, which is 20.8% lower than G-3, and the EL spectra of the three devices maintained basically unchanged (Fig. 5 (d)). We assume that the alkali metal has a stronger electron donating capacity, which is also consistent with the trend of their current density. Therefore, it is easier to cause the imbalance of carrier injection due to the special structure of IOLEDs. Accordingly, the IOLEDs have afforded excellent performance by initially optimizing the doping ratio of Ag doped Bphen as an EIL.

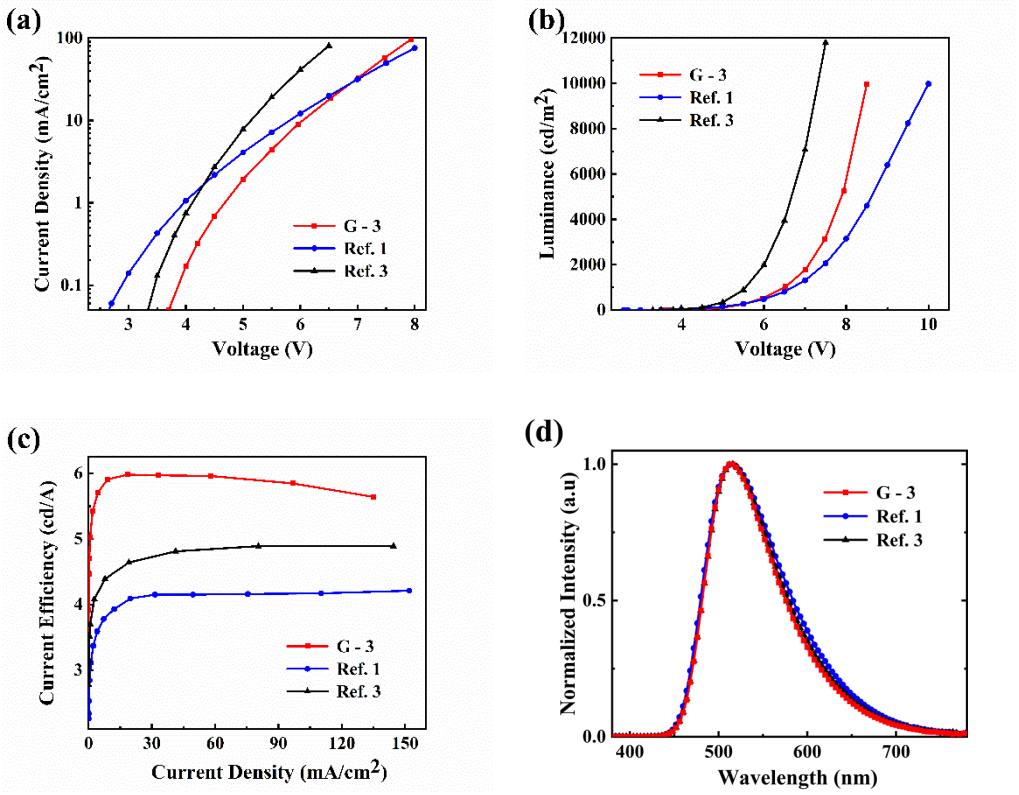

Fig. 5. The performance of OLEDs with different device structure. (a) Current density versus voltage (*J-V)*. (b) Luminance versus voltage (*L-V)*. (c) Current efficiency versus current density (*CE-J)* and (d) the corresponding EL spectra.

Next, we explored the effect of thermal annealing on the stability of blue fluorescent OLED with Cs_2CO_3 or Ag doped Bphen as an EIL. The materials used have higher T_g to eliminate other adverse effects. Figure 6s (a) and (b) show the current density and luminance changes of two blue IOLEDs with Cs_2CO_3 or Ag dopant annealed at different temperatures (RT, 60, 80 and 100 ℃) for one hour, respectively. After annealing increasing from RT to 80 °C, the current density and luminance of the device based on Cs_2CO_3-doped Bphen as an EIL decreased slightly, but still had good stability. However, its current density and luminance basically became zero when the temperature reached 100 °C, which is consistent with the results reported in the literature [11]. On the contrary, the current density and luminance of the IOLEDs based on Ag-doped Bphen after thermal annealing from RT to 100 °C show a tendency to increase first and then remain stable. As the annealing temperature rises reasonably, the carriers can overcome the interface energy barrier to increase the mobility, thus the current density will increase accordingly. This explains the increasing trend of the current density and luminance of the devices based on Ag-doped Bphen when the annealing temperature rises from RT to 60 ℃. During the process of rising the annealing temperature from 60 to 100 ℃, its current density and luminance remained unchanged basically, demonstrating its excellent thermal stability.

Furthermore, in order to further verify the thermal stability of Ag-doped Bphen as an EIL in blue IOLEDs, we investigated the changes in the current density (Fig. 6s (c)) and luminance (Fig. 6s (d)) properties of IOLEDs with different EILs versus annealing time at the annealing temperature of 100 ℃. The luminance of the device based on Cs_2CO_3-doped Bphen shows a sharp decline while its current density exhibits a trend of sharp decline first and then rises sharply. After annealing at 100 °C for 60 minutes, the current density of Cs_2CO_3-doped devices shows a sharp increase, resulting from the film crystallization or cracks, making the interface adjacent to EIL to break down. The thermal stability of the organic light-emitting diodes is closely related to the T_g of organic functional layers used in device. With the increase in the current density, the temperature within organic materials may be close to the T_g, leading to the change in the crystallization of organic materials. Therefore, the thermal-stability compound can effectively prevent the efficiency roll-off of the device. In addition, although B3PYMPM can hinder the diffusion of Cs^+ to a certain extent, the balance will be broken after a high temperature treatment at 100 °C, causing Cs^+ to diffuse into the EML, resulting in exciton quenching [33]. On the contrary, after annealing at 100 °C for 4 hours, the Ag-doped OLEDs still maintain excellent stability, in which its luminance remains stable after a certain increase while the current density increases slightly. The metal Ag or Cs will undergo a coordination reaction with Bphen to form a metal complex to improve the device performance and thermal stability [9,10].

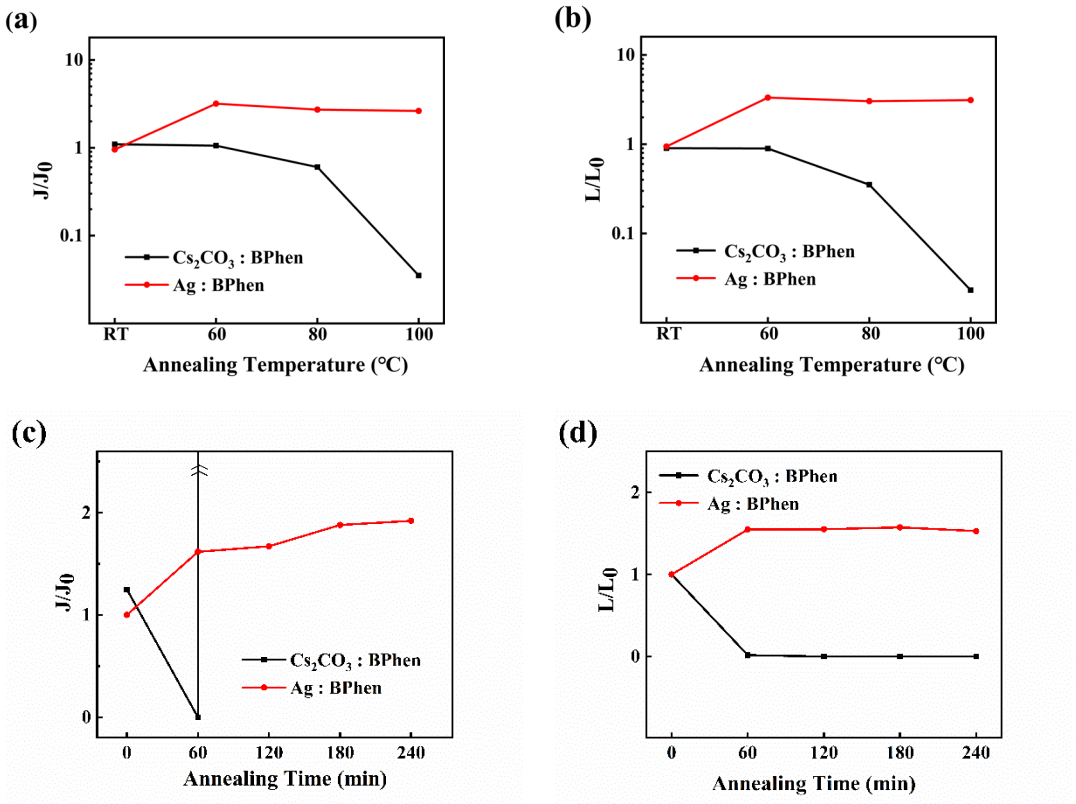

Fig. 6. The temporal evolution of current density (*J*) and luminance (*L*) at a 5 V bias voltage versus annealing temperature and time for the two types of blue IOLEDs with different EILs (10 wt% Ag or Cs_2CO_3: Bphen). The annealing time for both (a) and (b) is 60 min. The annealing temperature for both (c) and (d) is 100 ℃.

The difference in their thermal stability can be verified using an optical microscope to characterize the EML changes based on the different EILs versus different time under an annealing temperature of 100 °C. As shown in Fig. 7 (a), the light-emitting zone of the devices based on Ag-doped Bphen as an EIL have visible black spots and show a slow expansion, resulting from an excess amount of Ag particles. However, the emitting area of the blue IOLEDs based on Cs_2CO_3-doped Bphen is greatly reduced until the complete breakdown (Fig. 7 (b)). Therefore, the reasonable control of the doping

concentration and thickness can further improve the thermal stability of the device.

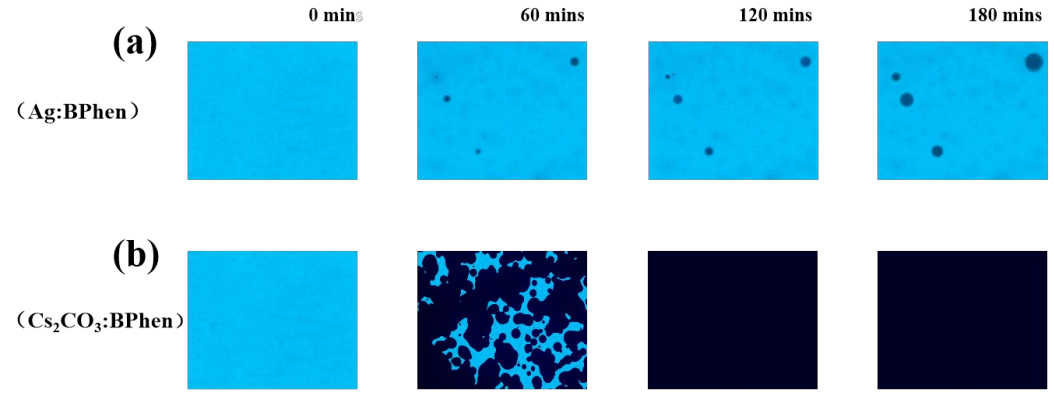

Fig. 7. The microscope images of emitting IOLEDs as a function of annealing times. (a) Blue IOLEDs based on Ag-doped Bphen. (b) Blue IOLEDs based on Cs_2CO_3-doped Bphen. The annealing temperature is 100 °C and the test is performed in an atmospheric environment.

4. Conclusions

In summary, IOLEDs based on Ag-doped Bphen can not only have excellent thermal stability, but also enhance photoelectrical properties. Importantly, the Bphen film with Ag dopants has higher thermal stability than both the neat Bphen and Cs_2CO_3-doped Bphen films. The mechanism of the Ag dopant in Bphen film was investigated by AFM and GISAXS. In addition, we confirm that Ag doped Bphen does have a more significant thermal stability than Cs_2CO_3 by studying the changes of the current density of EOCs and performance of the blue Ag-doped IOLEDs after annealing at different temperatures and time. Although the use of Cs_2CO_3 as a dopant can make the Bphen material maintain stable characteristics at 80 °C, Ag can play a more obvious role. Specifically, it can not only maintain the morphological stability of the Bphen matrix,

but also further improve the device performance after annealing at 100 °C for a long time. After annealing at 100 ℃ for 60 minutes, the film morphology of Ag doped BPhen film changed very little. Even if the annealing time reached 4 hours under the same condition, the brightness of the OLEDs with this configuration maintained unchanged basically. At the same time, for Ag-doped IOLEDs, we have achieved an amazing 20.8% enhancement in CE_{max} compared to the traditional IOLEDs with Cs_2CO_3 as an *n*-type dopant, even about 40.3% enhancement than the conventional device. This work can provide an alternative path for the commercial development of IOLEDs for the application in car taillights or others.

Acknowledgements

This work was financially supported by the National Natural Science Foundation of China (61775130, 11974236) and the Science and Technology Commission of Shanghai Municipality Program (19DZ2281000; 17DZ2281700). We acknowledge the beamline BL16B1 at Shanghai Synchrotron Radiation Facility for providing beam time. W.-Y. Wong thanks the Hong Kong Research Grants Council (PolyU 15305320), Guangdong-Hong Kong-Macao Joint Laboratory of Optoelectronic and Magnetic Functional Materials (2019B121205002), the Hong Kong Polytechnic University (1-ZE1C), Research Institute for Smart Energy (RISE) and the Endowed Professorship in Energy from Ms. Clarea Au (847S).

References

[1] C.W. Tang, S.A. VanSlyke, Organic electroluminescent diodes, Appl. Phys. Lett, 51 (1987) 913-915.

[2] Y. Miao, K. Wang, B. Zhao, L. Gao, P. Tao, X. Liu, Y. Hao, H. Wang, B. Xu, F. Zhu, High-efficiency/CRI/color stability warm white organic light-emitting diodes by incorporating ultrathin phosphorescence layers in a blue fluorescence layer, Nanophotonics, 7 (2018) 295-304.

[3] X. Zhou, M. Pfeiffer, J.S. Huang, J. Blochwitz-Nimoth, D.S. Qin, A. Werner, J. Drechsel, B. Maennig, K. Leo, Low-voltage inverted transparent vacuum deposited organic light-emitting diodes using electrical doping, Appl. Phys. Lett, 81 (2002) 922-924.

[4] T. Higuchi, H. Nakanotani, C. Adachi, High-efficiency white organic light-emitting diodes based on a blue thermally activated delayed fluorescent emitter combined with green and red fluorescent emitters, Adv Mater, 27 (2015) 2019-2023.

[5] H. Shin, J.H. Lee, C.K. Moon, J.S. Huh, B. Sim, J.J. Kim, Sky-Blue Phosphorescent OLEDs with 34.1% External Quantum Efficiency Using a Low Refractive Index Electron Transporting Layer, Adv Mater, 28 (2016) 4920-4925.

[6] A. Nathan, G.R. Chaji, S.J. Ashtiani, Driving Schemes for a-Si and LTPS AMOLED Displays, J. Disp. Technol, 1 (2005) 267-277.

[7] T. Riedl, P. Gorrn, W. Kowalsky, Transparent Electronics for See-Through AMOLED Displays, J. Disp. Technol, 5 (2009) 501-508.

[8] Y.H. Choi, Y.P. Jeon, D.C. Choo, T.W. Kim, Enhancement of out-coupling

efficiency due to an organic scattering layer in organic light-emitting devices, Org. Electro, 22 (2015) 197-201.

[9] Z. Bin, G. Dong, P. Wei, Z. Liu, D. Zhang, R. Su, Y. Qiu, L. Duan, Making silver a stronger n-dopant than cesium via in situ coordination reaction for organic electronics, Nat. Commun, 10 (2019) 866.

[10] Z. Bin, D. Shi, R. Su, W. Han, D. Zhang, L. Duan, Hydrogen bond modulation in 1,10-phenanthroline derivatives for versatile electron transport materials with high thermal stability, large electron mobility and excellent n-doping ability, Sci. Bull, 65 (2020) 153-160.

[11] C.-M. Keum, N.M. Kronenberg, C. Murawski, K. Yoshida, Y. Deng, C. Berz, W. Li, M. Wei, I.D.W. Samuel, M.C. Gather, The Role of Metallic Dopants in Improving the Thermal Stability of the Electron Transport Layer in Organic Light-Emitting Diodes, Adv. Opt. Mater, 6 (2018).

[12] Y. Cai, H.X. Wei, J. Li, Q.Y. Bao, X. Zhao, S.T. Lee, Y.Q. Li, J.X. Tang, Mechanism of Cs_2CO_3 as an n-type dopant in organic electron-transport film, Appl. Phys. Letters, 98 (2011).

[13] T. Earmme, S.A. Jenekhe, Solution-Processed, Alkali Metal-Salt-Doped, Electron-Transport Layers for High-Performance Phosphorescent Organic Light-Emitting Diodes, Adv. Funct. Mater, 22 (2012) 5126-5136.

[14] T. Ishida, H. Kobayashi, Y. Nakato, Structures and properties of electron-beam-evaporated indium tin oxide films as studied by x-ray photoelectron spectroscopy and work-function measurements, J. Appl. Phys, 73 (1993) 4344-4350.

[15] Q.-H. Wu, Progress in Modification of Indium-Tin Oxide/Organic Interfaces for Organic Light-Emitting Diodes, Crit. Rev. Solid. State, 38 (2013) 318-352.

[16] B.R. Lee, E.D. Jung, J.S. Park, Y.S. Nam, S.H. Min, B.S. Kim, K.M. Lee, J.R. Jeong, R.H. Friend, J.S. Kim, S.O. Kim, M.H. Song, Highly efficient inverted polymer light-emitting diodes using surface modifications of ZnO layer, Nat. Commun, 5 (2014) 4840.

[17] V. Thanikachalam, B. Seransenguttuvan, J. Jayabharathi, Efficient and chromaticity stable green and white organic light-emitting devices with organic–inorganic hybrid materials, RSC Adv, 10 (2020) 21206-21221.

[18] C.-l. Zhang, F.-c. Wang, Y. Zhang, H.-x. Li, S. Liu, Studying the Attribution of LiF in OLED by the - Characteristics, Int. J. Photoenergy, 2010 (2010) 1-4.

[19] J. Liu, Y. Li, S. Wang, Z. Ling, H. Lian, T. Xu, X. Zhang, Y. Liao, B. Wei, Long-lasting and efficient inverted pure blue organic light-emitting diodes by inserting an ultrathin aluminum interlayer, J. Alloy. Comp, 814 (2020).

[20] K. Guo, C. Si, C. Han, S. Pan, G. Chen, Y. Zheng, W. Zhu, J. Zhang, C. Sun, B. Wei, High-performance flexible inverted organic light-emitting diodes by exploiting MoS_2 nanopillar arrays as electron-injecting and light-coupling layers, Nanoscale, 9 (2017) 14602-14611.

[21] K. Guo, W. Li, J. Zhang, X. Zhang, X. Wang, G. Chen, T. Xu, L. Yang, W. Zhu, B. Wei, Extremely high external quantum efficiency of inverted organic light-emitting diodes with low operation voltage and reduced efficiency roll-off by using sulfide-based double electron injection layers, RSC Adv, 6 (2016) 55626-55634.

[22] S.-Y. Chen, T.-Y. Chu, J.-F. Chen, C.-Y. Su, C.H. Chen, Stable inverted bottom-emitting organic electroluminescent devices with molecular doping and morphology improvement, Appl. Phys. Lett, 89 (2006).

[23] C.-T. Tsai, P.-C. Kao, S.-Y. Chu, 2-Methyl-9,10-bis(naphthalen-2-yl)anthracene doped rubidium carbonate as an effective electron injecting interlayer on indium-tin oxide cathode in inverted bottom-emission organic light-emitting diodes, J. Appl. Phys, 124 (2018).

[24] Y. Chen, S. Chu, R. Li, Y. Qin, Y. Xu, X. Zhang, J. Wang, M. Liu, W.-Y. Lai, W. Huang, Highly efficient inverted organic light-emitting devices adopting solution-processed double electron-injection layers, Org. Electron, 66 (2019) 1-6.

[25] Y.Y. Tse, D. Babonneau, A. Michel, G. Abadias, Nanometer-scale multilayer coatings combining a soft metallic phase and a hard nitride phase: study of the interface structure and morphology, Surf. Coat. Tech, 180-181 (2004) 470-477.

[26] M. Buljan, S.R.C. Pinto, R.J. Kashtiban, A.G. Rolo, A. Chahboun, U. Bangert, S. Levichev, V. Holý, M.J.M. Gomes, Size and spatial homogeneity of SiGe quantum dots in amorphous silica matrix, J. Appl. Phys, 106 (2009).

[27] H.J. Kim, J.W. Kim, J.-J. Kim, Invited paper: Nanostructures of a mixed donor and acceptor layer in organic photovoltaics, Electron. Mater. Lett, 7 (2011) 93-104.

[28] J. Zhang, D. Posselt, D.M. Smilgies, J. Perlich, K. Kyriakos, S. Jaksch, C.M. Papadakis, Lamellar Diblock Copolymer Thin Films during Solvent Vapor Annealing Studied by GISAXS: Different Behavior of Parallel and Perpendicular Lamellae, Macromolecules, 47 (2014) 5711-5718.

[29] H. Sasabe, D. Tanaka, D. Yokoyama, T. Chiba, Y.-J. Pu, K.-i. Nakayama, M. Yokoyama, J. Kido, Influence of Substituted Pyridine Rings on Physical Properties and Electron Mobilities of 2-Methylpyrimidine Skeleton-Based Electron Transporters, Adv. Funct. Mater, 21 (2011) 336-342.

[30] H.I. Yang, S.H. Jeong, S.M. Cho, R. Lampande, K.-M. Lee, J.-A. Hong, J.-W. Choi, B.-s. Kim, Y. Park, R. Pode, J.H. Kwon, Efficient cathode contacts through Ag-doping in multifunctional strong nucleophilic electron transport layer for high performance inverted OLEDs, Org. Electron, 89 (2021).

[31] L. Zhou, H.Y. Xiang, Y.F. Zhu, Q.D. Ou, Q.K. Wang, J. Du, R. Hu, X.B. Huang, J.X. Tang, Multifunctional Silver Nanoparticle Interlayer-Modified ZnO as the Electron-Injection Layer for Efficient Inverted Organic Light-Emitting Diodes, ACS Appl. Mater. Inter, 11 (2019) 9251-9258.

[32] E. Rosenkrantz, S. Arnon, Local Surface Plasmon Tuning for Optical Devices, IEEE Photonic. Tech. L, 27 (2015) 669-672.

[33] Y.-H. Deng, Y.-Q. Li, Q.-D. Ou, Q.-K. Wang, F.-Z. Sun, X.-Y. Chen, J.-X. Tang, The doping effect of cesium-based compounds on carrier transport and operational stability in organic light-emitting diodes, Org. Electron, 15 (2014) 1215-1221.